Group VIII Metal Carbonyl Cluster-Boronic Acid Conjugates: Cytotoxicity and Mode of Action Studies

Jia Wen Kong,[⊥] Zhiyong Lam,[⊥] Kiat Hwa Chan, Rakesh Ganguly, Jia-Ying Joey Lee, Lit-Hsin Loo, Richard D. Webster, Zhen Xuan Wong, and Weng Kee Leong*

Cite This: ACS Omega 2021, 6, 29045−29053

Read Online

ACCESS | Metrics & More | Article Recommendations | Supporting Information

ABSTRACT: A set of metal carbonyl cluster-boronic acid conjugates of the group VIII metals (Fe, Ru, and Os) were synthesized and their antiproliferative effects measured against two breast cancer cell lines (MCF-7 and MDA-MB-231) and a noncancerous breast epithelial (MCF-10A) cell line. The cytotoxicity followed the order Ru > Os > Fe for the MDA-MB-231 cells, although the latter two exhibited similar cytotoxicity against MCF-7 and MCF-10A cells. The osmium species $\{Os_3(CO)_{10}(\mu\text{-H})[\mu\text{-SC}_6H_4\text{-}p\text{-B(OH)}_2]\}$ (2) could be chemically oxidized to its hydroxy analogue $[Os_3(CO)_{10}(\mu\text{-H})(\mu\text{-SC}_6H_4\text{-}p\text{-OH})]$ (2-OH), which showed comparable cytotoxicity. Mode of action studies pointed to an apoptotic pathway for cell death.

Apoptosis-Inducing
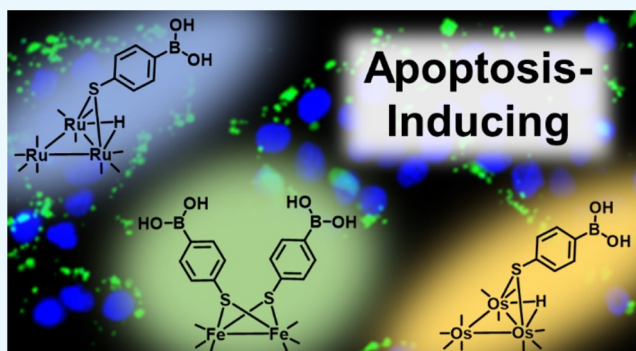
INTRODUCTION

Targeted cancer therapies, which involve blocking the growth and spread of cancer by interfering with specific molecular targets, are currently the focus of most anticancer drug development.[1,2] Such targeted therapies are designed to be specific for cancer over normal cells and are therefore likely to improve prognosis. Alterations in glycan expression are one of the hallmarks of malignant transformation, with the expression of sialic acid on the cell surface being one of the most widely reported.[3,4] Sialic acid is a class of N- or O-substituted neuraminic acid (a nine-carbon monosaccharide), and some common examples found on the terminal ends of glycans are N-acetylneuraminic acid (Neu5Ac) and 2-keto-3-deoxy-D-glycero-D-galacto-nononic acid (Kdn).[5] Overexpression of the enzymes N-acetylglucosaminyltransferase V and glycosyltransferase in cancer cells can lead to increased branching of the glycans and glycosylation at the terminal ends, respectively, resulting in an overall increase in sialylation.[6,7] Examples of glycan epitopes (parts of a protein for antibody recognition) commonly found in cancer cells include sialyl Lewis x (sLe^x) and polysialic acid.[8]

Boronic acids $[R\text{−B(OH)}_2]$ have been reported to interact with Neu5Ac at physiological pH (7.4), with a significantly higher binding constant than glucose.[9,10] This has spawned applications that utilize boronic acids to selectively target glycans on the surface of cancer cells, one interesting example being the use of a polymer functionalized with phenylboronic acid to selectively capture and release cancer cells that overexpress sialic acid.[11] Other work include the use of imaging agents, including quantum dots,[12] fluorescence

probe,[13] and gold nanoparticles,[14,15] that are functionalized with phenylboronic acid for the selective targeting and imaging of cancer cells. Boronic acids have also been used as functional and linker components to construct therapeutically useful bioconjugates.[16] There are also applications in medicinal chemistry; a number of boronic acid-containing drugs have been approved by the U.S. Food and Drug Administration (FDA) for medical use,[17] for example, Bortezomib and Ixazomib for the treatment of multiple myeloma.[18,19]

We have previously reported on a number of triosmium carbonyl clusters, in particular 1, which exhibited high cytotoxicity to both ER+ and ER- breast cancer cells.[20−22] More recently, we reported on a triosmium carbonyl cluster-boronic acid conjugate 2 for use in a specific and sensitive surface-enhanced Raman spectroscopy-based glucose assay (Figure 1).[23]

While conjugate 2 may potentially be used in cell-based and in vivo applications, such as, the identification of cancer cells via the binding of boronic acid to the surface glycans of the cells, it was found that this conjugate was cytotoxic toward the triple negative MDA-MB-231 breast carcinoma cell line.[24] The cytotoxicity of 2 may be attributed to the close proximity of the phenyl group to the metal core which allows a change in the
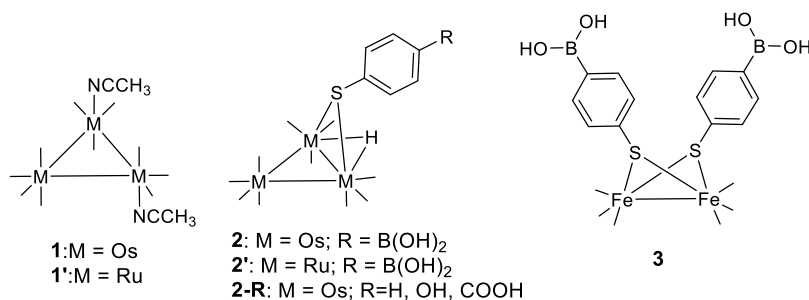
Figure 1. Molecular structures of metal carbonyl clusters **1**−**3** used in this study. Short lines denote carbonyl (CO) ligands.

bonding mode of the thiolate from μ-S-phenyl to an η^1-S-phenyl, thereby creating a vacant site on the osmium center for binding with biologically relevant targets.[24] In the present work, we have extended our investigations to the ruthenium and iron equivalents and some other related derivatives in an attempt to understand the effects of different group VIII metals on the cytotoxicity of the metal carbonyl cluster-boronic acid conjugates.

RESULTS AND DISCUSSION

The syntheses of the various clusters studied are depicted in Scheme 1. Cluster **2** was prepared in accordance to a

Scheme 1. Synthesis of Metal Carbonyl Clusters 1−3
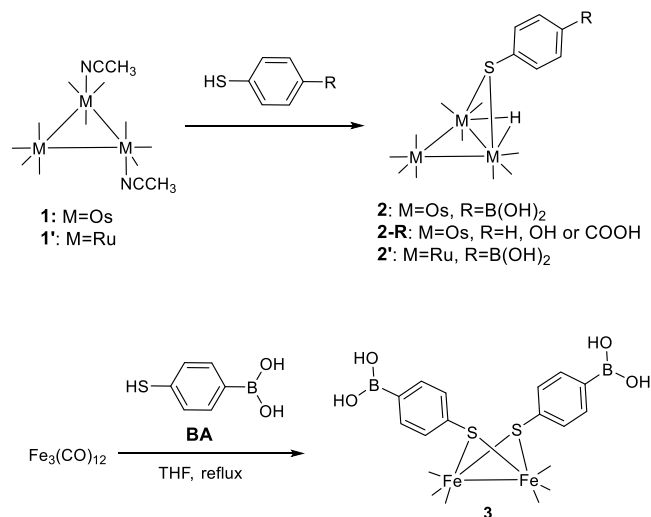
previously reported method.[23] As we envisaged that the boronic acid functionality of **2** may undergo oxidation to form the hydroxyl group in vivo,[25] the analogue **2-OH** was also synthesized and its structure confirmed crystallographically (Figure S2a).[26−28] The ruthenium homologue of **2**, viz., **2′**, was similarly synthesized from the reaction of $Ru_3(CO)_{10}(NCCH_3)_2$ (**1′**) with 4-mercaptophenylboronic acid (**BA**). The iron homologue of **2** is not accessible from the reaction of the monothiol with iron carbonyls; they tend to lead to diiron dithiolato carbonyl compounds.[29] Thus, cluster **3** was obtained from the reaction of $Fe_3(CO)_{12}$ with **BA** through modification of the reported methods.[29,30]

An attempt at a single-crystal X-ray crystallographic study of **2** afforded crystals which showed it to be the condensation trimer **4**, comprising a six-membered cluster-decorated boroxine ring (Figure 2). This is a common occurrence in the solid-state characterization of boronic acid moieties, but
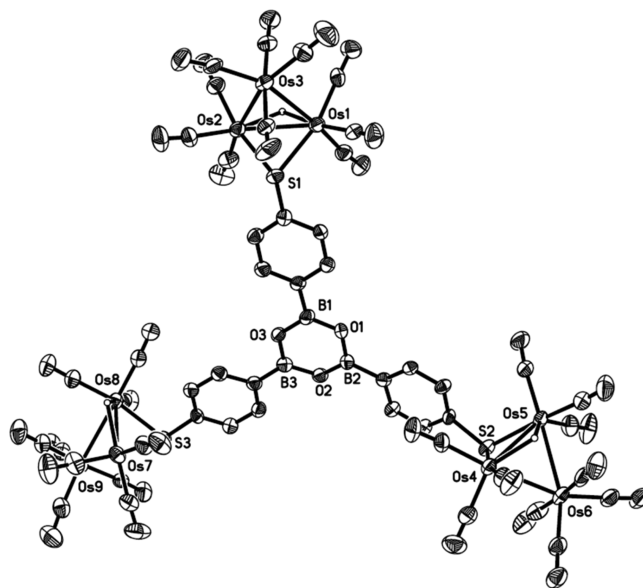

Figure 2. ORTEP plot of the molecular structure of condensation trimer **4**. Thermal ellipsoids are drawn at the 50% probability level.

boroxine is largely hydrolyzed in the presence of water to form the free boronic acid.[31] Although organometallic-decorated boroxines containing a triply ferrocene-bridged boroxine cyclophane have been reported,[32] to the best of our knowledge, this is the first example of a metal carbonyl-boroxine. The bond parameters of the $Os_3(\mu\text{-H})(\mu\text{-SR})$-$(CO)_{10}$ fragments in **4** are very similar to those for **2-OH** and **2-COOH** (Figure S1); the $Os(\mu-H)Os$ bond vector is longer than the unbridged Os−Os bonds, with an exception for one of the fragments of **4**.

The inhibition of cell proliferation by **2**, **2′**, and **3** was evaluated against the triple negative breast cancer cell line MDA-MB-231, the estrogen receptor positive (ER+) breast cancer cell line MCF-7, and the noncancerous breast epithelial cell line MCF-10A, with serum-free media (Table 1, Figure 3). Cluster **1** was used as the positive control, and the cytotoxicity of **BA** was also evaluated. The results indicated that free ligand **BA** is clearly not the source for the cytotoxicity but rather that the site of activity is the metal carbonyl cluster. The cytotoxicity followed the trend **2′** > **2** > **3** when tested against MDA-MB-231 cells. Cluster **2′** was also the most active against MCF-7 and MCF-10A cells, and clusters **2** and **3** appeared to have similar cytotoxicity. Unfortunately, there appeared to be no selectivity toward cancerous over the noncancerous cell line. It was also observed, as may be expected, that **2′** was not very stable, and hence, the subsequent studies were carried out on the osmium clusters.

Table 1. Inhibition of Cell Growth on Breast Cell Lines after 24 h under the Serum-free Condition, as Determined by the MTS Assay[a]

	$IC_{50}/\mu M$		
compounds	MDA-MB-231	MCF-7	MCF-10A
1	4.1 ± 0.5	7 ± 1	2.4 ± 0.4
BA	>50	>50	>50
2	3.5 ± 0.5	5.0 ± 0.7	2.6 ± 0.2
2′	0.37 ± 0.09	0.7 ± 0.2	0.5 ± 0.1
3	6 ± 1	5 ± 1	2.16 ± 0.04
2-OH	2.6 ± 0.4	3.1 ± 0.8	2.2 ± 0.5

[a]The experiments were carried out in triplicates with the standard errors obtained from at least two biological replicates.

The cytotoxicity of **2-OH**, a possible oxidation product of **2**, was also evaluated. Both **2-OH** and **2** exhibited similar cytotoxicity and were more active against MDA-MB-231 (ER-) than with MCF-7 (ER+) cells, suggesting that they were not acting via the estrogen receptors. Cell death was also verified visually with bright-field microscopy; significant changes to the cell morphology were observed in comparison to the negative control (Figure 3).

Interestingly, MTS assays on the compounds in the presence of serum suggest that although there was a substantial increase in the IC_{50} values, both **2** and **2-OH** were less susceptible to interference by serum than **1** which is known to interact with fetal bovine serum (FBS) (Table S1 and Figure S4);[20] the IC_{50} of **1** increased 7−8 folds in the presence of serum, which is higher than the 2−5 fold increase for **2** and **2-OH** (Figure S4).[21] The interference in **1** has been attributed to its reactivity with thiol and carboxylic acid residues in serum proteins to

form stable μ-S and μ,κ^2-O,O′ clusters, respectively.[21,27,28,33] It is this chemical reactivity of **1** which allowed the conjugation of triosmium clusters onto biomolecules.[34] The lower degree of serum interference with **2** and **2-OH** therefore suggests that they are intrinsically more chemically stable and hence may be better drug candidates than **1**.

The oxidation of boronic acid by H_2O_2 to form the hydroxyl group is the basis for BA and boronate ester-based sensors in H_2O_2 sensing (Scheme 2).[25,35−37] The conversion of **2** into **2-**

Scheme 2. Oxidation of Boronic Acid or Boronate Ester by H_2O_2
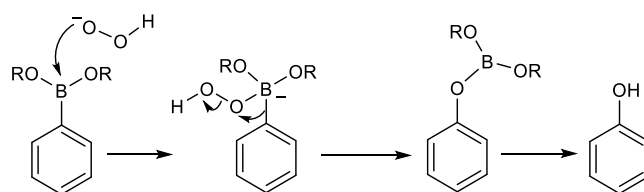
OH in the presence of H_2O_2, with imidazole as the base, was confirmed by IR spectroscopy (Figure S5). The shift in the CO vibrational bands to a lower wavenumber was indicative of the conversion to **2-OH** and verified against an authentic sample. Monitoring the reaction by ESI-HRMS also showed a decline in the ratio of **2** (m/z 1004) to **2-OH** (m/z 976) over time (Figure S6); a control without the addition of H_2O_2 showed a consistent high ratio of the peak at 1004 to that at 976 throughout the reaction, indicating little or no loss of **2**. Thus, cluster **2** could be oxidized chemically to **2-OH**; it is therefore possible that this could happen intracellularly. The lipophilicity of the compounds, as measured by their log $P_{o/w}$ values,
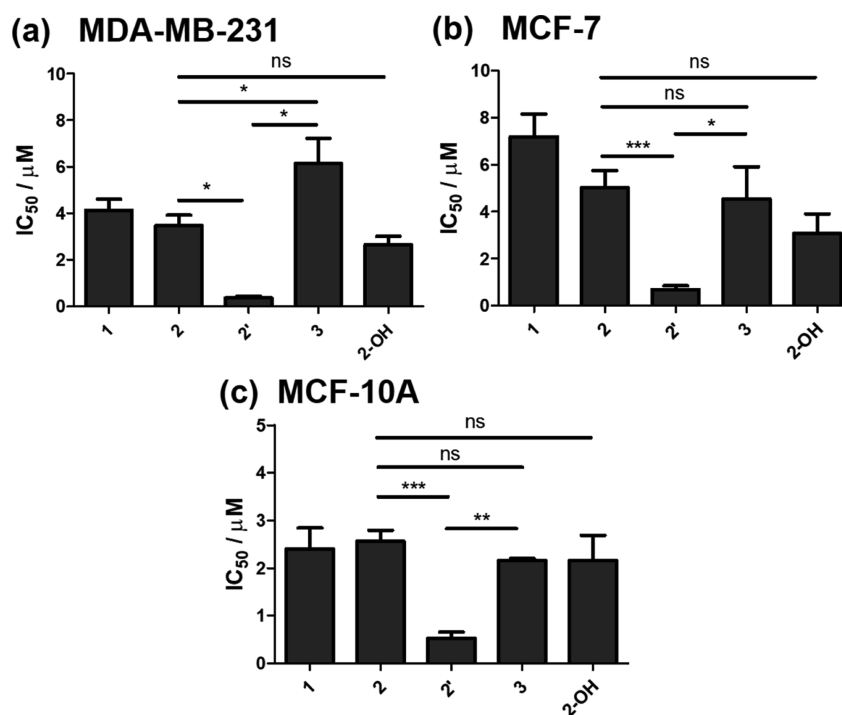
Figure 3. Comparison of the IC_{50} of **1**, **2**, **2′**, **3**, and **2-OH** on the following: (a) MDA-MB-231; (b) MCF-7; and (c) MCF-10A cells after 24 h under the serum-free condition, as determined by the MTS assay. The experiments were carried out in triplicates with the standard errors obtained from at least two biological replicates. Statistical analysis was performed by unpaired t-test with $p < 0.05$ considered significant (*$p < 0.05$, **$p < 0.01$, ***$p < 0.001$, ns: not significant).
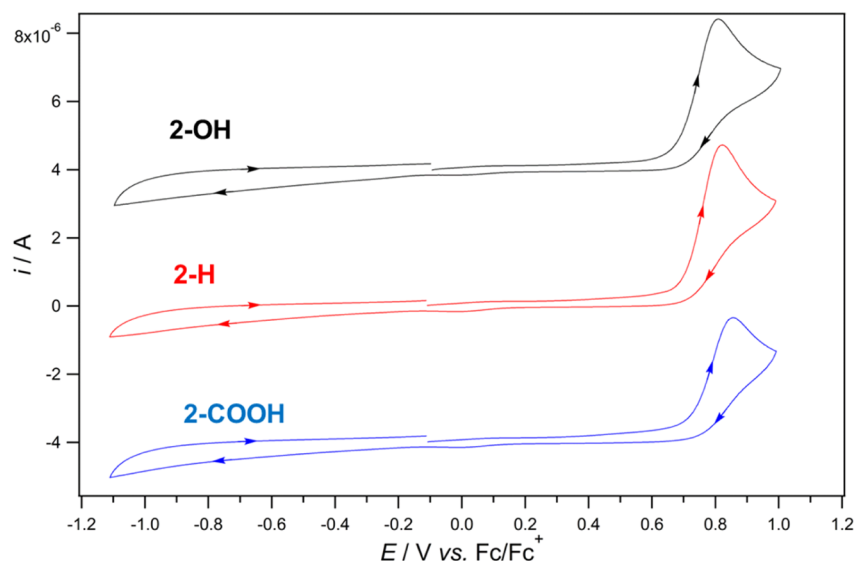
Figure 4. Cyclic voltammograms of **2-OH**, **2-H**, and **2-COOH** in acetonitrile (2 mM) at 22 ± 0.2 °C with 0.1 M $n\text{Bu}_4\text{NPF}_6$, recorded on a 1 mm diameter planar glassy carbon electrode at a scan rate of 0.1 V s^{-1}.
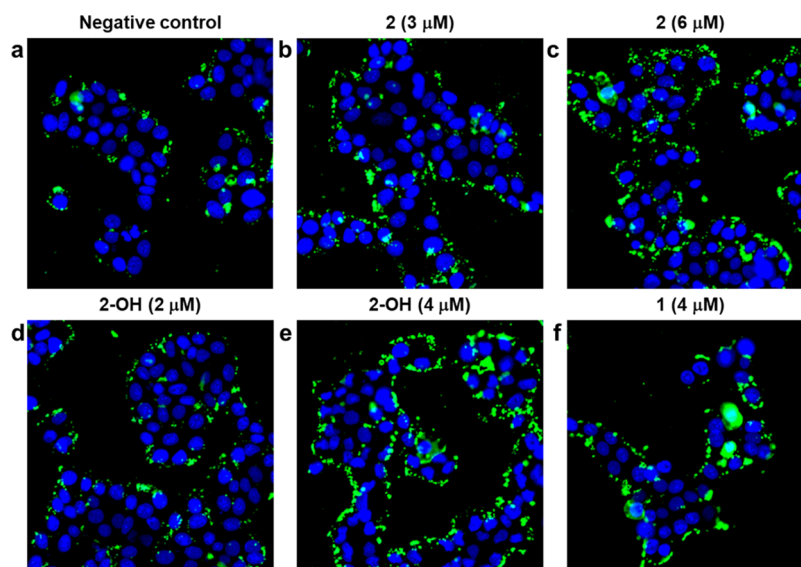

Figure 5. Fluorescence images of MCF-7 cells stained with Hoechst 33342 (blue) and Annexin V-FITC (green) after a 20 h treatment with the following: (a) negative control, 0.5% DMSO (v/v); (b,c) **2** (3 and 6 μM, respectively); (d,e) **2**-OH (2 and 4 μM, respectively); and (f) **1** (4 μM). Cells treated with **2**, **2-OH**, and **1** showed a higher amount of Annexin V-FITC staining than the negative control.

followed the order **2-COOH** > **2** > **2-OH** (Table S2). We attribute this rather unexpected trend to the formation of H-bonded dimers or oligomers in **2-COOH** and **2**.[38−41] The fact that the cytotoxicity of all three clusters do not differ significantly suggests little correlation with their lipophilicity.

The structure of **2-OH** (i.e. phenol group) is reminiscent of organometallic-based anticancer drugs such as ferrocifen (a ferrocenyl derivative of tamoxifen) in which a ferrocene-modulated phenol oxidation to the reactive quinone methide is believed to be responsible for its cytotoxicity.[42−44] We thus investigated the electrochemical behavior of **2-OH** by cyclic voltammetry (CV) with $n\text{Bu}_4\text{NPF}_6$ as the supporting electrolyte, in comparison with the phenyl and carboxylic analogues **2-H** and **2-COOH** (Figure 4). These clusters showed irreversible oxidation at 0.80, 0.82, and 0.85 V (vs Fc/Fc$^+$) for **2-OH**, **2-H**, and **2-COOH**, respectively. The fact that the oxidation potential appears to be quite independent of the

functional group on the phenyl ring suggests that oxidation is at the triosmium cluster core. The corresponding reduction is not observed in the reverse scan, pointing to an unstable oxidized species, which is in agreement with reports that oxidation of the triosmium pyridyl cluster $[\text{Os}_3(\mu\text{-H})\text{-}(\text{CO})_{10}(\mu\text{-NC}_5\text{H}_4)]$ and analogues is irreversible.[45] It is thus unlikely that the cytotoxicity of **2-OH** is due to phenol oxidation, as has been observed with ferrocifen.

The induction of apoptosis by **2** and **2-OH** as the cause of cell death was established in experiments with MCF-7 cells. Fluorescence microscopy of cells treated with **1**, **2**, and **2-OH** for 20 h and subsequently stained with Hoechst 33342 showed nuclei of reduced size and distorted shape, a sign of early apoptosis. Cells with nuclei showing chromatin condensation were also observed, similar to those in the positive control (cluster **1**) and in contrast to those in the negative control [0.5% dimethyl sulfoxide (DMSO), v/v] which had round and
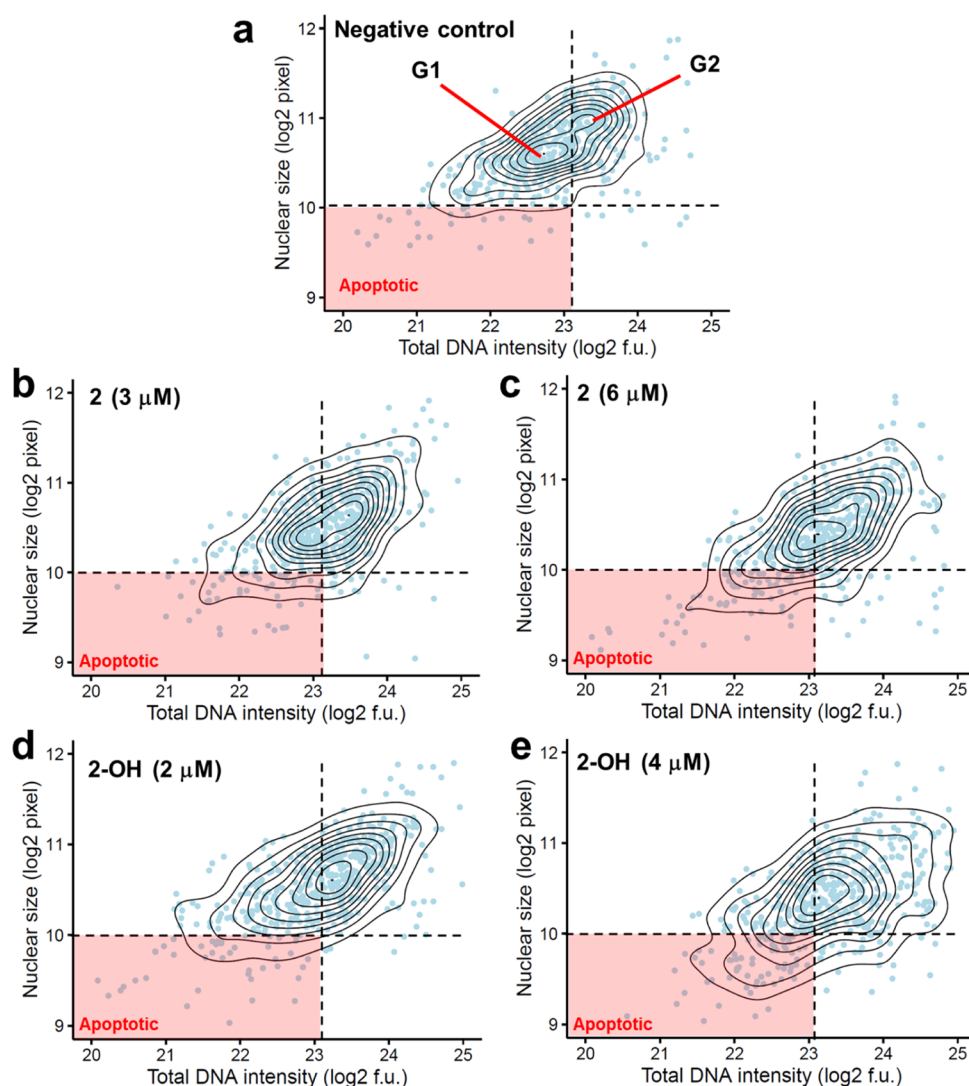
Figure 6. Contour-scatter plots showing the nuclear area vs total DNA fluorescence intensity of single MCF-7 cells after a 20 h treatment: (a) negative control, 0.5% DMSO (v/v); (b,c) **2** (3 and 6 μM, respectively); and (d,e) **2-OH** (2 and 4 μM, respectively). The dots represent single-cell measurements quantified from the images.

intact nuclei (Figure S7). Apoptosis leads to the externalization of phosphatidylserine at the cell surface, which can be stained with Annexin V-fluorescein isothiocyanate (FITC).[46−48] MCF-7 cells treated with **1**, **2**, and **2-OH** and stained with Hoechst 33342 and Annexin V-FITC showed a significant increase in Annexin V-FITC staining (green) in comparison to the negative control (Figure 5). The intensity also increased with treatment at higher concentrations; image-based quantification of the membrane (non-DNA region) also showed substantial Annexin V-FITC staining with the increase in concentration (Figure S8).

Changes in the nuclear morphology were also quantified through image-based single cell phenotypic analysis of the nuclear area and fluorescence intensity of the cell population.[49] Fluorescence images were segmented into single cells with the relevant cellular features extracted for quantification.[50] This well-established technique has already been used in a high-throughput image-based nephro- and pulmonary toxicity prediction platform for toxic compounds.[51,52] Apoptotic cells generally display reduced nuclear area and fluorescence intensity in comparison to normal cells. MCF-7 cells treated with increasing concentrations of both **2** and **2-OH** resulted in

an increased population of cells with smaller nuclear size and lower DNA intensity (lower left quadrant of the contour-scatter plots) in comparison to the negative control; this is consistent with apoptosis (Figure 6). While the contour plot for the negative control showed two distinct cell populations characterized by the G1 and G2 phases of the cell cycle, respectively (Figure 6a), treatment with the clusters resulted in a shift in the cell population to the G2 phase (top right quadrant) which may suggest G2/M arrest; the cells were not able to undergo mitosis.

■ CONCLUSIONS

In this work, we synthesized and compared the cytotoxicity of three metal carbonyl cluster-boronic acid conjugates of the group VIII metals (Fe, Ru, and Os) against two breast cancer cell lines (MCF-7 and MDA-MB-231) and a noncancerous breast epithelial (MCF-10A) cell line. The cytotoxicity followed the order: Ru > Os > Fe for the identity of the metal, with MDA-MB-231 cells; the latter two were comparable in cytotoxicity against MCF-7 and MCF-10A. We have also shown that the osmium cluster **2** could be

chemically oxidized to its hydroxyl analogue **2-OH**, and both clusters induced cell death via an apoptotic pathway. Work is underway to make improvements toward selectivity in this class of metal carbonyl clusters and to understand their mode of action in greater detail.

■ EXPERIMENTAL SECTION

General Experimental Section. All reactions and manipulations were carried out under an argon atmosphere using standard Schlenk techniques. Solvents that were used for reaction were distilled over the appropriate drying agents under argon before use. Purification of compounds was generally carried out by column chromatography on silica gel, or by preparative thin-layer chromatography (TLC) using 20 cm × 20 cm plates precoated with silica gel 60 F_{254}. Infrared (IR) spectra were recorded on a Bruker Alpha Fourier transform infrared spectrometer. Solution spectra were recorded in DCM solution, unless otherwise stated, in a solution IR cell with NaCl or CaF_2 (for MeOH solutions) windows and a path length of 0.1 mm, at a resolution of 2 cm^{-1}. ^1H NMR spectra were recorded on a JEOL ECA 400 or ECA 400SL (400 MHz) spectrometer in $(CD_3)_2CO$ and chemical shifts are referenced to the residual proton resonance of the solvent. High-resolution mass spectrometry (HRMS) spectra were recorded in the ESI mode on a Waters UPLC-Q-TOF MS mass spectrometer. High-performance liquid chromatography (HPLC) measurements were carried out with an Agilent Technologies 1220 Infinity LC Model equipped with a diode array detector controlled by Agilent LC 1220 OpenLAB software. $Os_3(CO)_{12}$ was purchased from Oxkem Ltd, and all other reagents from other commercial sources and used as supplied without further purification. The clusters **1**, **1′**, **2-H**, **2-OH**, and **2-COOH** were synthesized according to reported procedures with slight modifications;[26−28,53,54] the structures of the latter two were also confirmed by X-ray crystallography. Cluster **2** was synthesized according to a reported procedure[23] and characterized crystallographically as condensation trimer **4**.

Synthesis of 2′. Cluster **1′** (approx. 104 mg, 0.156 mmol) was prepared following a slight modification of the literature method in acetonitrile/DCM,[54] filtered through silica gel cold (∼−20 to 0 °C), and then, 4-mercaptophenylboronic acid (36 mg, 0.234 mmol) was added. The mixture was stirred for 90 min at room temperature, the solvent removed under vacuum, and the residue separated by preparative TLC with ethyl acetate/hexane (1:1, v/v) as the eluent. The band at R_f = 0.50 was recovered to afford **2′**. Yield = 29.6 mg (25.7%). IR (cm^{-1}): ν_{CO} 2105 (w), 2066 (s), 2058 (m), 2024 (s), 2009 (sh), 1992 (w). ^1H NMR: δ 7.80 (2H, d, J = 8.5, Ar), 7.43 (2H, d, J = 8.6, Ar), 7.28 (s, 2H, B(O$\underline{H}$)$_2$), −14.92 (s, 1H, Ru$\underline{H}$Ru). ESI-HRMS (m/z): 653.6997; calcd for $C_{13}H_7BO_9SRu_3$ [M − 3(CO)]$^-$: 653.7033.

Synthesis of 3. A solution of $Fe_3(CO)_{12}$ (50 mg, 0.099 mmol) and 4-mercaptophenylboronic acid (34 mg, 0.218 mmol) in dry THF (5 mL) was heated at reflux for 30 min. The solvent was then removed under vacuum, and the residue was separated by preparative TLC with acetonitrile/DCM (1:1, v/v) as the eluent. The band at R_f = 0.71 was recovered and recrystallized from acetone/hexane to give **3**. Yield = 7.9 g (14%). IR (cm^{-1}): ν_{CO} 2076 (m), 2040 (vs), 2000 (s). ^1H NMR: δ 7.75−7.70 (4H, m, Ar), 7.42−7.38 (4H, m, Ar), 7.25 (s, 2H, B(O$\underline{H}$)$_2$), 7.22 (s, 2H, B(OH)$_2$). ESI-HRMS (m/z): 584.8736.; calcd for $C_{18}H_{11}B_2O_{10}S_2Fe_2$ [M − H]$^-$: 584.8679.

Chemical Oxidation of 2. A solution of **2** (4.4 mg, 0.0044 mmol) dissolved in MeOH (3 mL) was added to imidazole (1 equiv) dissolved in deionized water. Hydrogen peroxide solution (2.2 μL, 30% w/w) was added to the mixture and left to incubate at room temperature over 3 h. For analysis by IR spectroscopy, an aliquot of the mixture was removed and dried under a stream of nitrogen. The yellow residue was dissolved in MeOH and analyzed by IR spectroscopy in a CaF_2 IR solution cell. For ESI-HRMS analysis, the mixture was diluted with MeOH prior to analysis.

Lipophilicity. The octanol−water partition coefficients (log $P_{o/w}$) were measured by reversed-phase HPLC with a C8 (Phenomenex Luna, 25 cm × 4.6 mm i.d., 5 μm) according to the method described by Minick.[55] Test samples were dissolved in methanol and diluted to 0.1 μM, with the exception of **2** which was diluted to 1 μM. The chromatographic capacity factor (k_ϕ) for each compound was measured at various fractions (ϕ), in the range 70−85%, of methanol (containing 0.25% octanol) and an aqueous phase of 1-octanol-saturated water containing n-decylamine (0.15%, v/v) and 3-morpholinopropanesulfonic acid (0.02 M) at pH 7.4. The column dead time was taken as the solvent disturbance peak for each run.[56] The log k_ϕ values were extrapolated to 100% of the aqueous component to give the log k_w values from which log $P_{o/w}$ values were then obtained with the formula log $P_{o/w}$ = 0.13418 + 0.98452 log k_w.

Cell Culture. Experimental cultures of breast (MDA-MB-231, MCF-7, and MCF-10A) were obtained from the American Type Culture Collection (ATCC) and cultured in tissue culture dishes (Corning, NY) at 37 °C in 5% CO_2 atmosphere. Phosphate-buffered saline was obtained from Gibco. Experiments were performed on cells within 20 passages. The breast cancer cells MDA-MB-231 and MCF-7 cells were maintained in Dulbecco's modified Eagle's medium (DMEM; Biowest L0106, France) supplemented with 10% FBS (Gibco, NY), 1% L-glutamine (PAA Laboratories, Austria), and 1% penicillin/streptomycin (HyClone, UT). The MCF-10A cells were maintained in a DMEM-F12 medium (Biowest L0093, France) supplemented with 7.5% FBS (Gibco, NY), epidermal growth factor (Invitrogen), insulin (Sigma-Aldrich), hydrocortisone (Sigma-Aldrich) and 0.4% gentamicin (Gibco, NY), and 1% penicillin/streptomycin (HyClone, UT). Bright-field images of the adhered cells were taken using a Nikon Eclipse TS100 inverted microscope, with a 10× objective and Nikon digital Sight DS-L3 camera.

Cell Proliferation Assay. The antiproliferation activity of the compounds on the various cell lines was screened using the MTS assay modified from those reported previously.[20,22] Stock solutions of the compounds in sterile-filtered DMSO or ethanol were prepared and serial diluted to lower concentrations. For treatment with the compounds, cells were seeded into 96-well plates in serum-supplemented medium at the same initial density of 10 000 cells (80 μL) per well and allowed to adhere and grow for 24 h. For serum-free experiments, the cells were allowed to adhere and grow for 18 h followed by serum-starving in serum-free medium for 6 h before treatment with the indicated concentrations of compounds in a serum-free medium (0.5% DMSO or ethanol) for 24 h. Control cells were treated with vehicle (0.5% DMSO or ethanol). To each well, 10 μL of MTS reagent (MTS Cell Proliferation Assay Kit, BioVision, CA) was added and then left to incubate in a 37 °C incubator with 5% CO_2 for 2 h. The absorbance intensities at 490 nm were then measured, and the

cell proliferation relative to the control sample was calculated. Each sample was analyzed in triplicates and was corrected with background intensities from same incubation conditions without the cells. IC_{50} was determined from a sigmoidal dose response (variable slope) equation using GraphPad Prism 5 software. The values were obtained from at least two (up to seven) separate experiments with the mean value and standard error calculated. Statistical analysis was done by Student's unpaired *t*-test using GraphPad Prism 5 software.

Apoptosis Assay. MCF-7 cells were seeded into 96-well optical-grade glass black plates with transparent bottom (Nunc Inc, IL), precoated with fibronectin (0.5%, Santa Cruz Biotechnology) in a serum-supplemented medium at the same initial density of 10 000 cells (80 μL) per well, and allowed to adhere and grow for 18 h. This was followed by serum-starving in a serum-free medium for 6 h before treatment with the indicated concentrations of compounds in serum-free medium (0.5% DMSO) for 20 h. Control cells were treated with vehicle (0.5% DMSO). Three replicates were performed for each treatment condition. Apoptotic/necrotic/ healthy cells detection kit (PromoKine, Heidelberg, Germany) was used to identify apoptotic cells. The adhered cells were washed twice with 1× binding buffer (2 × 50 μL), followed by staining with Hoechst 33342 and Annexin V-FITC at room temperature for 15 min. The stained cells were washed twice with 1× binding buffer (2 × 50 μL) before proceeding to imaging in the buffer (70 μL).

Image Acquisition, Segmentation, and Feature Extraction. Fluorescence imaging was performed with a 20× objective using the Axio Observer Z1 (Zeiss), with coolSNAP HQ2 (Photometrics, SONY) camera and Definite laser focus (Zeiss) focusing system. Nine sites per well were imaged. The images were saved in the 16-bit TIFF format and corrected using the "rolling ball" algorithm implemented in ImageJ (NIH, v1.48) to reduce nonuniform background illuminations.[57] Cell segmentations and feature measurements were performed using the cellXpress software platform (Bioinformatics Institute, A*STAR, v1.4).[50]

Cyclic Voltammetry. CV experiments were performed with a computer-controlled Eco Chemie Autolab PGSTAT302N potentiostat in a three-electrode cell with a 1 mm diameter planar glassy carbon (GC) disk working electrode (Cypress Systems), a Pt auxiliary electrode (Metrohm), and an Ag wire miniature reference electrode (Cypress Systems) which was connected to the test solution via a salt bridge containing 0.5 M nBu$_4$NPF$_6$ in CH$_3$CN. Ferrocene (Fc) was used as an internal standard at the end of the measurements. All solutions used for the voltammetric experiments were deoxygenated by purging with argon gas and measurements were performed in a Faraday cage.

X-ray Crystallographic Analysis. Diffraction-quality single crystals were obtained by the slow evaporation of solutions: **2** in toluene and **2-OH** and **2-COOH** in DCM. The crystals were mounted onto quartz fibers, and diffraction intensity data were collected on a Bruker κ diffractometer equipped with a charge-coupled device detector and using Mo Kα radiation (λ = 0.71073 Å), with the SMART suite of programs.[58] Data were processed and corrected for Lorentz and polarization effects with SAINT and for absorption effects with SADABS.[59] Structural solution and refinement were performed with the SHELXTL suite of programs.[60]

The crystals of **2-OH** were found to be twinned; the twin law and cell parameters were determined using the program CELL_NOW,[61] and the reflection data were processed and corrections applied using the program TWINABS.[62] The structures were solved by direct methods to locate the heavy atoms, followed by successive difference maps for the light, nonhydrogen atoms. Solvates were found in all three crystals— two positions (one with occ = 0.25) for DCM in **2-OH**, one DCM in **2-COOH**, and two positions for toluene (one at a special position with occ = 0.80 and disordered) in **4**. Appropriate restraints were placed on the disordered parts. All nonhydrogen atoms were refined with anisotropic thermal parameters in the final model. The metal hydrides were located using low-angle difference maps, while organic hydrogen atoms were placed in calculated positions; they were assigned isotropic thermal parameters and refined with a riding model. The crystallographic data for the structures are summarized in Table S3..

■ ASSOCIATED CONTENT

Ⓢ Supporting Information

The Supporting Information is available free of charge at https://pubs.acs.org/doi/10.1021/acsomega.1c04116.

> Characterization data and biochemical assay results (PDF)

> Crystallographic data for compound **2-COOH** has been deposited with the Cambridge Crystallographic Data Centre as supplementary publication number CCDC# 2069170 (CIF)

> Crystallographic data for compound **2-OH** has been deposited with the Cambridge Crystallographic Data Centre as supplementary publication number CCDC# 2069172 (CIF)

> Crystallographic data for compound **4** has been deposited with the Cambridge Crystallographic Data Centre as supplementary publication number CCDC# 2069171 (CIF)

■ AUTHOR INFORMATION

Corresponding Author

Weng Kee Leong − *Division of Chemistry and Biological Chemistry, School of Mathematical and Physical Sciences, Nanyang Technological University, Singapore 637371, Singapore;* Ⓞ orcid.org/0000-0003-3198-7111; Email: chmlwk@ntu.edu.sg

Authors

Jia Wen Kong − *Division of Chemistry and Biological Chemistry, School of Mathematical and Physical Sciences, Nanyang Technological University, Singapore 637371, Singapore*

Zhiyong Lam − *Division of Chemistry and Biological Chemistry, School of Mathematical and Physical Sciences, Nanyang Technological University, Singapore 637371, Singapore*

Kiat Hwa Chan − *Yale-NUS College, Singapore 138527, Singapore*

Rakesh Ganguly − *Division of Chemistry and Biological Chemistry, School of Mathematical and Physical Sciences, Nanyang Technological University, Singapore 637371, Singapore;* Present Address: NH91, Tehsil Dadri, Greater Noida, Gautam Buddha Nagar, Shiv Nadar University, India 201314; Ⓞ orcid.org/0000-0002-9523-6918

Jia-Ying Joey Lee − *Agency for Science, Technology, and Research (A*STAR), Bioinformatics Institute (BII), Singapore 138671, Singapore*

Lit-Hsin Loo − *Agency for Science, Technology, and Research (A*STAR), Bioinformatics Institute (BII), Singapore 138671, Singapore; Department of Pharmacology, Yong Loo Lin School of Medicine, National University of Singapore, Singapore 119077, Singapore;* orcid.org/0000-0001-6303-9840

Richard D. Webster − *Division of Chemistry and Biological Chemistry, School of Mathematical and Physical Sciences, Nanyang Technological University, Singapore 637371, Singapore;* orcid.org/0000-0002-0896-1960

Zhen Xuan Wong − *Division of Chemistry and Biological Chemistry, School of Mathematical and Physical Sciences, Nanyang Technological University, Singapore 637371, Singapore*

Complete contact information is available at:
https://pubs.acs.org/10.1021/acsomega.1c04116

Author Contributions

[⊥]J.W.K. and Z.L. contributed equally.

Notes

The authors declare no competing financial interest.

■ REFERENCES

(1) Targeted Cancer Therapies. https://www.cancer.gov/about-cancer/treatment/types/targeted-therapies/targeted-therapies-fact-sheet#what-are-targeted-cancer-therapies (accessed 10 Jan 2021).

(2) Troy, A. B. Targeted Cancer Therapy: The Next Generation of Cancer Treatment. *Curr. Drug Discovery Technol.* **2015**, *12*, 3−20.

(3) Büll, C.; Stoel, M. A.; den Brok, M. H.; Adema, G. J. Sialic Acids Sweeten a Tumor's Life. *Cancer Res.* **2014**, *74*, 3199−3204.

(4) Dube, D. H.; Bertozzi, C. R. Glycans in cancer and inflammation - potential for therapeutics and diagnostics. *Nat. Rev. Drug Discovery* **2005**, *4*, 477−488.

(5) Varki, A.; Schauer, R., Sialic Acids. In *Essentials of Glycobiology*, 2nd edition, Varki, A., Cummings, R. D.; Esko, J. D.; Freeze, H. H.; Stanley, P.; Bertozzi, C. R.; Hart, G. W.; Etzler, M. E., Eds.; Cold Spring Harbor: Cold Spring Harbor Laboratory Press: NY, 2009.

(6) Dennis, J.; Laferte, S.; Waghorne, C.; Breitman, M.; Kerbel, R. Beta 1-6 branching of Asn-linked oligosaccharides is directly associated with metastasis. *Science* **1987**, *236*, 582−585.

(7) Kim, Y. J.; Varki, A. Perspectives on the significance of altered glycosylation of glycoproteins in cancer. *Glycoconjugate J.* **1997**, *14*, 569−576.

(8) Orntoft, T. F.; Vestergaard, E. M. Clinical aspects of altered glycosylation of glycoproteins in cancer. *Electrophoresis* **1999**, *20*, 362−371.

(9) Otsuka, H.; Uchimura, E.; Koshino, H.; Okano, T.; Kataoka, K. Anomalous Binding Profile of Phenylboronic Acid with N-Acetylneuraminic Acid (Neu5Ac) in Aqueous Solution with Varying pH. *J. Am. Chem. Soc.* **2003**, *125*, 3493−3502.

(10) Djanashvili, K.; Frullano, L.; Peters, J. A. Molecular Recognition of Sialic Acid End Groups by Phenylboronates. *Chem.—Eur. J.* **2005**, *11*, 4010−4018.

(11) Liu, H.; Li, Y.; Sun, K.; Fan, J.; Zhang, P.; Meng, J.; Wang, S.; Jiang, L. Dual-Responsive Surfaces Modified with Phenylboronic Acid-Containing Polymer Brush To Reversibly Capture and Release Cancer Cells. *J. Am. Chem. Soc.* **2013**, *135*, 7603−7609.

(12) Liu, A.; Peng, S.; Soo, J. C.; Kuang, M.; Chen, P.; Duan, H. Quantum Dots with Phenylboronic Acid Tags for Specific Labeling of Sialic Acids on Living Cells. *Anal. Chem.* **2010**, *83*, 1124−1130.

(13) Xu, X.-D.; Cheng, H.; Chen, W.-H.; Cheng, S.-X.; Zhuo, R.-X.; Zhang, X.-Z. In situ recognition of cell-surface glycans and targeted imaging of cancer cells. *Sci. Rep.* **2013**, *3*, 2679.

(14) Lin, L.; Tian, X.; Hong, S.; Dai, P.; You, Q.; Wang, R.; Feng, L.; Xie, C.; Tian, Z.-Q.; Chen, X. A Bioorthogonal Raman Reporter Strategy for SERS Detection of Glycans on Live Cells. *Angew. Chem., Int. Ed.* **2013**, *52*, 7266−7271.

(15) Yin, D.; Wang, S.; He, Y.; Liu, J.; Zhou, M.; Ouyang, J.; Liu, B.; Chen, H.-Y.; Liu, Z. Surface-enhanced Raman scattering imaging of cancer cells and tissues via sialic acid-imprinted nanotags. *Chem. Commun.* **2015**, *51*, 17696−17699.

(16) António, J. P. M.; Russo, R.; Carvalho, C. P.; Cal, P. M. S. D.; Gois, P. M. P. Boronic acids as building blocks for the construction of therapeutically useful bioconjugates. *Chem. Soc. Rev.* **2019**, *48*, 3513−3536.

(17) Plescia, J.; Moitessier, N. Design and discovery of boronic acid drugs. *Eur. J. Med. Chem.* **2020**, *195*, 112270.

(18) Kane, R. C.; Farrell, A. T.; Sridhara, R.; Pazdur, R. United States Food and Drug Administration Approval Summary: Bortezomib for the Treatment of Progressive Multiple Myeloma after One Prior Therapy. *Clin. Cancer Res.* **2006**, *12*, 2955−2960.

(19) Shirley, M. Ixazomib: First Global Approval. *Drugs* **2016**, *76*, 405−411.

(20) Kong, K. V.; Leong, W. K.; Ng, S. P.; Nguyen, T. H.; Lim, L. H. K. Osmium Carbonyl Clusters: A New Class of Apoptosis Inducing Agents. *ChemMedChem* **2008**, *3*, 1269−1275.

(21) Kong, K. V.; Leong, W. K.; Lim, L. H. K. Osmium Carbonyl Clusters Containing Labile Ligands Hyperstabilize Microtubules. *Chem. Res. Toxicol.* **2009**, *22*, 1116−1122.

(22) Lee, H. Z. S.; Leong, W. K.; Top, S.; Vessières, A. Cytotoxic Triosmium Carbonyl Clusters: A Structure-Activity Relationship Study. *ChemMedChem* **2014**, *9*, 1453−1457.

(23) Kong, K. V.; Lam, Z.; Lau, W. K. O.; Leong, W. K.; Olivo, M. A Transition Metal Carbonyl Probe for Use in a Highly Specific and Sensitive SERS-Based Assay for Glucose. *J. Am. Chem. Soc.* **2013**, *135*, 18028−18031.

(24) Koh, W. X.; Coppo, L.; Holmgren, A.; Kong, J. W.; Leong, W. K. Inhibition of Thioredoxin Reductase by Triosmium Carbonyl Clusters. *Chem. Res. Toxicol.* **2020**, *33*, 2441−2445.

(25) Simon, J.; Salzbrunn, S.; Surya Prakash, G. K.; Petasis, N. A.; Olah, G. A. Regioselective Conversion of Arylboronic Acids to Phenols and Subsequent Coupling to Symmetrical Diaryl Ethers. *J. Org. Chem.* **2001**, *66*, 633−634.

(26) Crooks, G. R.; Johnson, B. F. G.; Lewis, J.; Williams, I. G. The chemistry of polynuclear compounds. Part XVI. Trinuclear thiol derivatives of dodecacarbonyl-triruthenium and -triosmium. *J. Chem. Soc. A* **1969**, 797−799.

(27) Ainscough, E. W.; Brodie, A. M.; Coll, R. K.; Mair, A. J. A.; Waters, J. M. Linked triosmium cluster complexes containing thiolato-carboxylato ligands: the crystal and molecular structures of [{Os3H-(CO)10}2(μ-SC6H4CO2)] and [{Os3H(CO)10}2(μ-SCH2CH2CO2)]. *J. Organomet. Chem.* **1996**, *509*, 259−264.

(28) Li, C.; Leong, W. K. The reaction of triosmium and -ruthenium clusters with bifunctional ligands. *J. Organomet. Chem.* **2008**, *693*, 1292−1300.

(29) Li, Y.; Rauchfuss, T. B. Synthesis of Diiron(I) Dithiolato Carbonyl Complexes. *Chem. Rev.* **2016**, *116*, 7043−7077.

(30) Thomas, C. M.; Rüdiger, O.; Liu, T.; Carson, C. E.; Hall, M. B.; Darensbourg, M. Y. Synthesis of Carboxylic Acid-Modified [FeFe]-Hydrogenase Model Complexes Amenable to Surface Immobilization. *Organometallics* **2007**, *26*, 3976−3984.

(31) Korich, A. L.; Iovine, P. M. Boroxine chemistry and applications: A perspective. *Dalton Trans.* **2010**, *39*, 1423−1431.

(32) Chen, T.-H.; Kaveevivitchai, W.; Bui, N.; Miljanić, O. Š. Triply ferrocene-bridged boroxine cyclophane. *Chem. Commun.* **2012**, *48*, 2855−2857.

(33) Ainscough, E. W.; Brodie, A. M.; Coll, R. K.; Coombridge, B. A.; Waters, J. M. The reaction of $[Os_3(CO)_{10}(CH_3CN)_2]$ with carboxylic acids: the crystal and molecular structures of $[Os_3H-(CO)_{10}(C_6H_4(OH)CO_2)]$ and $[Os_3H(CO)_{10}(C_6H_5COS)]$. *J. Organomet. Chem.* **1998**, *556*, 197−205.

(34) Kong, K. V.; Chew, W.; Lim, L. H. K.; Fan, W. Y.; Leong, W. K. Bioimaging in the Mid-Infrared Using an Organometallic Carbonyl Tag. *Bioconjugate Chem.* **2007**, *18*, 1370−1374.

(35) Lippert, A. R.; Van de Bittner, G. C.; Chang, C. J. Boronate Oxidation as a Bioorthogonal Reaction Approach for Studying the Chemistry of Hydrogen Peroxide in Living Systems. *Acc. Chem. Res.* **2011**, *44*, 793−804.

(36) Miller, E. W.; Albers, A. E.; Pralle, A.; Isacoff, E. Y.; Chang, C. J. Boronate-Based Fluorescent Probes for Imaging Cellular Hydrogen Peroxide. *J. Am. Chem. Soc.* **2005**, *127*, 16652−16659.

(37) Dickinson, B. C.; Chang, C. J. Chemistry and biology of reactive oxygen species in signaling or stress responses. *Nat. Chem. Biol.* **2011**, *7*, 504−511.

(38) Chen, J.; Brooks, C. L.; Scheraga, H. A. Revisiting the Carboxylic Acid Dimers in Aqueous Solution: Interplay of Hydrogen Bonding, Hydrophobic Interactions, and Entropy. *J. Phys. Chem. B* **2008**, *112*, 242−249.

(39) Tzeli, D.; Theodorakopoulos, G.; Petsalakis, I. D.; Ajami, D.; Rebek, J. Theoretical Study of Hydrogen Bonding in Homodimers and Heterodimers of Amide, Boronic Acid, and Carboxylic Acid, Free and in Encapsulation Complexes. *J. Am. Chem. Soc.* **2011**, *133*, 16977−16985.

(40) Larkin, J. D.; Bhat, K. L.; Markham, G. D.; Brooks, B. R.; Schaefer, H. F.; Bock, C. W. Structure of the Boronic Acid Dimer and the Relative Stabilities of Its Conformers. *J. Phys. Chem. A* **2006**, *110*, 10633−10642.

(41) Cyrański, M. K.; Jezierska, A.; Klimentowska, P.; Panek, J. J.; Sporzyński, A. Impact of intermolecular hydrogen bond on structural properties of phenylboronic acid: quantum chemical and X-ray study. *J. Phys. Org. Chem.* **2008**, *21*, 472−482.

(42) Hillard, E.; Vessières, A.; Thouin, L.; Jaouen, G.; Amatore, C. Ferrocene-Mediated Proton-Coupled Electron Transfer in a Series of Ferrocifen-Type Breast-Cancer Drug Candidates. *Angew. Chem., Int. Ed.* **2006**, *45*, 285−290.

(43) Plażuk, D.; Vessières, A.; Hillard, E. A.; Buriez, O.; Labbé, E.; Pigeon, P.; Plamont, M.-A.; Amatore, C.; Zakrzewski, J.; Jaouen, G. A [3]Ferrocenophane Polyphenol Showing a Remarkable Antiproliferative Activity on Breast and Prostate Cancer Cell Lines. *J. Med. Chem.* **2009**, *52*, 4964−4967.

(44) Jaouen, G.; Vessières, A.; Top, S. Ferrocifen type anti cancer drugs. *Chem. Soc. Rev.* **2015**, *44*, 8802−8817.

(45) Wong, W.-Y.; Wong, W.-T. Synthesis, redox behaviour and molecular structures of new metal cluster species containing orthometallated $[M_3(\mu\text{-}H)(CO)10(\mu\text{-}NC5H4)]$ (M = Ru or Os) and ferrocene chromophores bridged by an aromatic unit. *J. Chem. Soc., Dalton Trans.* **1996**, *15*, 3209−3214.

(46) Lee, S.-H.; Meng, X. W.; Flatten, K. S.; Loegering, D. A.; Kaufmann, S. H. Phosphatidylserine exposure during apoptosis reflects bidirectional trafficking between plasma membrane and cytoplasm. *Cell Death Differ.* **2013**, *20*, 64−76.

(47) Zwaal, R. F. A.; Comfurius, P.; Bevers, E. M. Surface exposure of phosphatidylserine in pathological cells. *Cell. Mol. Life Sci.* **2005**, *62*, 971−988.

(48) van Genderen, H.; Kenis, H.; Lux, P.; Ungeth, L.; Maassen, C.; Deckers, N.; Narula, J.; Hofstra, L.; Reutelingsperger, C. In vitro measurement of cell death with the annexin A5 affinity assay. *Nat. Protoc.* **2006**, *1*, 363−367.

(49) Loo, L.-H.; Wu, L. F.; Altschuler, S. J. Image-based multivariate profiling of drug responses from single cells. *Nat. Methods* **2007**, *4*, 445−453.

(50) Laksameethanasan, D.; Tan, R. Z.; Toh, G. W.-L.; Loo, L.-H. cellXpress: a fast and user-friendly software platform for profiling cellular phenotypes. *BMC Bioinf.* **2013**, *14*, S4.

(51) Su, R.; Xiong, S.; Zink, D.; Loo, L.-H. High-throughput imaging-based nephrotoxicity prediction for xenobiotics with diverse chemical structures. *Arch. Toxicol.* **2016**, *90*, 2793−2808.

(52) Lee, J.-Y. J.; Miller, J. A.; Basu, S.; Kee, T.-Z. V.; Loo, L.-H. Building predictive in vitro pulmonary toxicity assays using high-throughput imaging and artificial intelligence. *Arch. Toxicol.* **2018**, *92*, 2055−2075.

(53) Nicholls, J. N.; Vargas, M. D.; Deeming, A. J.; Kabir, S. E. Some Useful Derivatives of Dodecacarbonyltriosmium. *Inorg. Synth.* **1989**, *26*, 289−293.

(54) Grenouillet, P.; de Bellefon, C. Coordination chemistry of mono- and di-nitriles in $[Ru_3(CO)_{12\text{-}n}(RCN)_n]$ (n = 1−3): influence of the CO/nitrile ratio on fluxionality. *J. Organomet. Chem.* **1996**, *513*, 155−162.

(55) Minick, D. J.; Frenz, J. H.; Patrick, M. A.; Brent, D. A. A comprehensive method for determining hydrophobicity constants by reversed-phase high-performance liquid chromatography. *J. Med. Chem.* **1988**, *31*, 1923−1933.

(56) Knox, J. H.; Kaliszan, R. Theory of solvent disturbance peaks and experimental determination of thermodynamic dead-volume in column liquid chromatography. *J. Chromatogr. A* **1985**, *349*, 211−234.

(57) Sternberg, S. R. Biomedical Image Processing. *Computer* **1983**, *16*, 22−34.

(58) *SMART*, version 5.628; Bruker AXS Inc., Madison, WI, USA, 2001.

(59) Sheldrick, G. M. *SADABS*; University of Göttingen: Göttingen, Germany, 1996.

(60) *SHELXTL*, version 5.1; Bruker AXS Inc., Madison, WI, USA, 1997.

(61) Sheldrick, G. M. *CELL_NOW*; University of Göttingen: Göttingen, Germany, 2008.

(62) Sheldrick, G. M. *TWINABS*; University of Göttingen: Göttingen, Germany, 2008.